Avrupa Bilim ve Teknoloji Dergisi
Sayı 52, S. 122-135, Kasım 2023

Araştırma Makalesi

www.ejosat.com ISSN:2148-2683

European Journal of Science and Technology
No. 52, pp. 122-135, November 2023

Research Article

Theoretical Insights into the Effects of Positional Isomerism: DFT/TD-DFT Approach

Sümeyya Serin[1]*, Öznur Doğan Ulu[2]

[1*] Scientific and Technological Research Center, İnonu University, Malatya, Türkiye, (ORCID: 0000-0002-4637-1734), sumeyya.alatas@inonu.edu.tr
[2] Scientific and Technological Research Center, İnonu University, Malatya, Türkiye, (ORCID: 0000-0002-5561-227X), oznur.dogan@inonu.edu.tr

(İlk Geliş Tarihi 5 Ağustos 2023 ve Kabul Tarihi 15 Ekim 2023)

(**DOI:** 10.5281/zenodo.10259308)

ATIF/REFERENCE: Serin, S., Doğan Ulu, Ö. (2023). Theoretical Insights into the Effects of Positional Isomerism: DFT/TD-DFT Approach. *Avrupa Bilim ve Teknoloji Dergisi*, (52), 122-135.

Abstract

The phenomenon of positional isomerism arises when functional groups or substituents occupy different positions in the same carbon skeleton. Although the molecular formula remains the same, the arrangement of atoms in the molecule is different. This leads to differences in physical and chemical properties. In this context, the present study aims to investigate the properties of the three isomers (**1-3**) obtained from the interaction of 3-formylacetylacetone with ortho-, meta- and para-aminobenzoic acids using computational chemistry methods. Density Functional Theory (DFT) studies were carried out to explore the effects of positional isomerism on thermodynamic parameters, physicochemical quantities, reactivity indices, electrostatic surface properties and intramolecular interactions. All calculations in the study were carried out using the GAUSSIAN 16 software package by applying the B3LYP functional and the 6-311++G (d, p) basis set. Also, the TD-DFT method was used in order to examine ground and excited state characteristics. No significant changes were observed in the computed ΔE (total energy), ΔH (enthalpy), and ΔG (Gibbs free energy) values of all three isomers. On the other hand, as a result of the frontier molecular orbital analysis, it was determined that the quantum chemical reactivity descriptors differed.

Keywords: Positional Isomerism, Aminobenzoic Acid, DFT, Reactivity.

Konumsal İzomerizmin Etkilerine İlişkin Teorik Görüşler: DFT/TD-DFT Yaklaşımı

Öz

Fonksiyonel grupların veya sübstitüentlerin aynı karbon iskeletinde farklı konumları işgal etmesiyle konumsal izomerizm olgusu ortaya çıkmaktadır. Moleküler formül aynı kaldığı halde molekül içindeki atomların dizilişi farklıdır. Bu durum fiziksel ve kimyasal özelliklerde farklılıklara yol açar. Bu bağlamda, mevcut çalışma, 3-formilasetilasetonun orto-, meta- ve para-aminobenzoik asitlerle etkileşiminden elde edilen üç izomerin (**1-3**) özelliklerinin hesaplamalı kimya yöntemleri kullanılarak incelenmesini amaçlamaktadır. Konumsal izomerinin, termodinamik parametreler, fizikokimyasal büyüklükler, reaktivite indisleri, elektrostatik yüzey özellikleri ve molekül içi etkileşimler üzerindeki etkilerini araştırmak için Yoğunluk Fonksiyonel Teori (YFT) çalışması yapıldı. Çalışmada yer alan tüm hesaplamalar, B3LYP fonksiyoneli ve 6-311++G (d, p) temel seti uygulanarak GAUSSIAN 16 yazılım paketi kullanılarak gerçekleştirilmiştir. Ayrıca, temel ve uyarılmış durum özelliklerini incelemek için TD-DFT yöntemi kullanılmıştır. Her üç izomerin hesaplanan ΔE (toplam enerji), ΔH (entalpi) ve ΔG (Gibbs serbest enerjisi) değerlerinde kaydadeğer değişikler gözlenmemiştir. Buna karşın, sınır moleküler orbital analizi sonucunda kuantum kimyasal reaktivite tanımlayıcılarının farklılık gösterdiği belirlenmiştir.

Anahtar Kelimeler: Konumsal İzomerizm, Aminobenzoik Asit, YFT, Reaktivite**.**

* Corresponding Author: sumeyya.alatas@inonu.edu.tr

1. Introduction

Organic reactions involving the condensation of different molecules to synthesize new compounds are very important in candidate drug design. The azomethine group, also known as Schiff bases, containing (C=N) as a functional group, are condensation products formed as a result of the reaction of primary amines and aldehydes or ketones. These compounds have applications in many fields such as organometallic chemistry, industrial, photography and textile (Gogoi et al., 2022). In addition, due to their biological properties, they are used very effectively in medicinal chemistry such as antioxidant (Singh et al., 2022), antibacterial (Ardakani et al., 2018), antifungal, and anticancer (Tadele et al., 2019). This compound, which was not known until the 19th century, was recognized in coordination chemistry, and attracted a lot of attention not only with its biological activities, but also with the complexes it formed with metals. Many studies have been conducted on both the synthesis and characterization of Schiff base metal complexes and their applications in different fields. For example, Yin et al. (2012) reported the DNA binding properties of Schiff base-based organotin complexes. Similarly, the synthesis of the Cu complex of Schiff base was reported by Niu et al. (2011), while the prepared ONO Schiff base ligand and the biological activities of Cu(II), Zn(II) and Cd(II) complexes were studied by Gogoi et al. (2022). In a study reported by Halz et al., new Schiff bases were synthesized from the reaction of different isomers of aminobenzoic acid with 3-formylacetylacetone and their structures were also determined by X-ray single crystal diffraction (Halz et al., 2022). There are strong intramolecular N-H…O hydrogen bridge in the structures of the synthesized compounds. Due to the position of the carboxyl, the synthesized molecules exhibit the positional isomerism. The relative position of the substituents in a molecule is one of the critical factors affecting its physicochemical properties. The critical role of positional isomerism has been documented in various fields of the chemical sciences (Eliel and Wilen, 1994). In a study by Chen et al., they have reported two new potentially energetic melt-castable molecules that are a pair of positional isomers. They demonstrated both experimentally and theoretically the effects of the positional isomerism on properties such as density, melting point, decomposition temperature, and stability. The aforementioned study drew attention to the importance of developing positional isomerization for superior performance in the design of new energetic materials (Chen et al., 2023). In another study, the effects of positional isomerism on the mesophase behavior of two newly synthesized liquid crystal series were investigated. (Vyas et al., 2022). It has been demonstrated that the different twist angles as a result of the change in the positions of the substituents have affected the transition enthalpy values of the series. In addition, Aadhityan et al., investigated the spin-dependent electron transport properties of 4,6-dibromobenzene-1,3-dithiol, 2,4-dibromobenzene-1,3-dithiol, and 2,5-dibromobenzene-1,3-dithiol isomers. They also supported the findings with theoretical studies (Aadhityan et al., 2021). Related work highlights the importance of an atom's position in the spin-dependent electronic transport properties of dibromobenzene isomers to find efficient molecular junction. Thus, studies on positional isomers reveal the possibility of improving a molecular property of interest by selecting an appropriate isomer. Based on these considerations, it is becoming more significant to explore the effects of positional isomerism on molecules. The use of quantum chemical computation methods in this laborious exploration process provides a great advantage to researchers as it will ensure the opportunity to evaluate it numerically and visually. Therefore, in this study, it is aimed to deal with the specified *ortho* (**1**), *meta* (**2**), and *para* (**3**) isomers from a quantum chemical point of view. In this context, the effects of positional isomerism in terms of physicochemical properties, reactivity behaviors, intramolecular interactions, and electrostatic surface properties are discussed by performing DFT-based calculations. It is expected that the findings obtained from this study will be efficient in guiding further research on the relevant isomers. Besides, the research results are important in terms of providing new insights into the effects of the positional isomerism.

2. Computational Methodology

All optimization and frequency computations presented in the study were performed by using GAUSSIAN 16 software package (Frisch et al., 2016) on applying the B3LYP method and the 6-311++G (d, p) basis set to realize the optimized structures of **1-3** (Becke, 1993; Lee et al., 1988; Becke, 1993). Gauss View 6 software (Dennington et al., 2016) was utilized for illustrations of the optimized structures, FMO, and MEP diagrams. To gain the density of states (DOS) plots, Gauss-Sum 3.0 (O'Boyle et al., 2008) program was operated. The solvent phase calculations (acetonitrile and water) were carried out by using solvation model based on density (SMD) (Marenich et al., 2009).

The thermochemical quantities, $E_{vib.}$, $S_{vib.}$, and $Cv_{vib.}$ of the studied isomers were computed through specific equations ((1)-(5)) defined below in accordance with the principles of quantum mechanics (McQuarrie,1973; Hill, 1962; Herzberg, 1964; Serdaroğlu, 2010). The following explanations refer to the terms presented in the eqns: $\Theta_{v,j}=h\nu_j /k\rightarrow$ vibrational temperature, k→ Boltzmann constant, h→ Planck constant, and νj→ j^{th} fundamental frequency.

$$Q = Q_{trans.} \times Q_{rot.} \times Q_{vib.} Q_{elec.} \quad (1)$$

$$Q_{vib.} = \prod_{j=1}^{3N-6} \frac{e^{-\Theta_{v,j}/2T}}{\left(1 - e^{-\frac{\Theta_{v,j}}{T}}\right)} \quad (2)$$

$$E_{vib.} = Nk \sum_{j=1}^{3N-6} \left(\frac{\Theta_{v,j}}{2} + \frac{\Theta_{v,j}\, e^{-\,\Theta_{v,j}/T}}{\left(1 - e^{-\frac{\Theta_{v,j}}{T}}\right)} \right) \quad (3)$$

$$S_{vib.} = Nk \sum_{j=1}^{3N-6} \left[\frac{\Theta_{v,j}/T}{\left(e^{\Theta_{v,j}/T} - 1\right)} - \ln\left(1 - e^{-\Theta_{v,j}/T}\right) \right] \quad (4)$$

$$Cv_{vib.} = Nk \sum_{j=1}^{3N-6} \left[\left(\frac{\Theta_{v,j}}{T}\right)^2 \frac{e^{\Theta_{v,j}/T}}{\left(e^{\Theta_{v,j}/T} - 1\right)^2} \right] \quad (5)$$

According to Koopmans theorem (Koopmans, 1934), ionization energy (I) and electron affinity (A) values can be defined by Highest Occupied Molecular Orbital (HOMO) and Lowest Unoccupied Molecular Orbital (LUMO) energies. Moreover, some DFT-based reactivity parameters such as chemical hardness (η), chemical potential (μ), electronegativity (χ), electrophilicity index (ω), maximum charge transfer capability index (ΔN_{max}), back-donation energy ($\Delta E_{back\text{-}donation}$), electron-accepting power (ω+), and electron-donating power (ω-) as well as frontier molecular orbital energies (E_{HOMO} and E_{LUMO}) are presented in the equations below ((6)-(13)) (Parr and Pearson , 1983; Pearson, 1986; Parr, 1999; Perdew and Levy, 1983; Perdew et al., 1982; Gazquez et al., 2007; Gomez et al., 2006).

$$\mu = -\frac{I + A}{2} \quad (6)$$

$$\eta = \frac{I - A}{2} \quad (7)$$

$$\chi = \frac{I + A}{2} \quad (8)$$

$$\omega = \frac{\mu^2}{2\eta} \quad (9)$$

$$\omega^+ \approx (I + 3A)^2/(16(I - A)) \quad (10)$$

$$\omega^- \approx (3I + A)^2/(16(I - A)) \quad (11)$$

$$\Delta N_{max} = \frac{I + A}{2(I - A)} \quad (12)$$

$$\Delta\varepsilon_{back-donation} = -\frac{\eta}{4} \quad (13)$$

NBO analyses of the **1-3** were carried out utilizing the second-order Fock matrix (Weinhold et al., 2016; Reed et al., 1988) at DFT/B3LYP/6–311++G (d, p) methodology. In this way, donor-acceptor orbital interactions and stabilization energy estimations were defined. Energy values were computed via formula specified in equation (14). The symbols in the formula can be expressed as follows: $E^{(2)}$: Stabilization energy, qi: Donor orbital occupancy, Fij: Off diagonal Fock matrix, εi and εj: diagonal element, donor and acceptor orbital energies.

$$E^{(2)} = \Delta E_{ij} = qi\left[\frac{(Fij)^2}{(\varepsilon j - \varepsilon i)}\right] \quad (14)$$

3. Results and Discussion

3.1. Molecular Structure

Three positional isomers **1, 2,** and **3** were optimized by DFT/B3LYP/6–311++G (d, p) methodology. The three-dimensional structures of the optimized, numbered and labeled compounds are illustrated in Figure 1. It has been reported that the derivative **1** crystallizes in the monoclinic system (C2/*c* space group), the derivative **2** in the orthorhombic system (*Pnma* space group), and the derivative **3** in the monoclinic system ($P2_1/c$ space group) (Halz et al., 2022). Also, Table 1 represents some selected geometrical parameters of studied compounds with corresponding experimental values) (Halz et al., 2022).

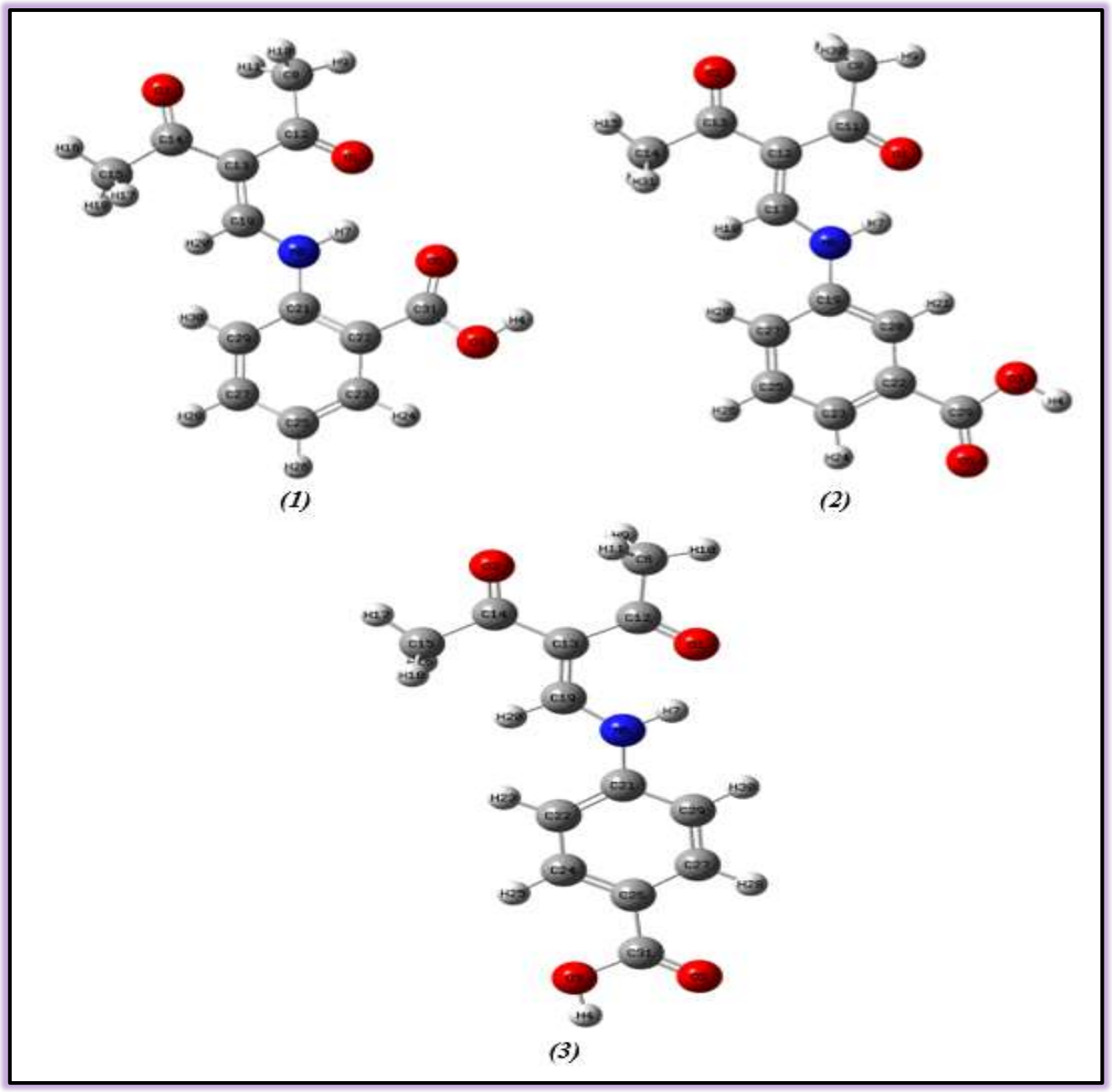

Figure 1. The optimized structures of studied molecules in the gas phase

According to Table 1, O1-C12 bond distances were computed as 1.231 Å for compound **1** and 1.239 Å for compound **3**. On the other hand, in compound **2**, the O1-C11 bond length corresponding to the same bond was calculated as 1.239 Å. Similarly, O2-C14 bond distances were defined as 1.222 Å for both compounds **1** and **3**. It was estimated as 1.222 Å for O2-C13, which is its equivalent in compound **2**. The angles of C19-N6-C21, N6-C19-C13, and O1-C12-C8 of compound **1** were estimated as 124.4°, 127.5°, and 118.9°, respectively, while these angles were computed as 127.8°, 125.6°, and 118.3° for compound **3**. The equivalents of the mentioned angles in compound **2** were calculated as 127.8°, 125.7°, and 118.3°, respectively. Considering the dihedral angles, similar results were obtained for compounds **1** and **3**. The N6-C21-C22-C23 dihedral angle of **1** was calculated as 178.8°, while in **3**, the angle of N6-C21-C22-C24 corresponding to the same angle was predicted as 179.9°. In addition, obtaining the dihedral angles of compound **2** as 0.0° and 180.0° supports the exact planarity. As demonstrated in Table 1, the values computed for compounds **1**-**3** are in good agreement with the X-ray data.

*Table 1. Some selected structural parameters of **1-3***

Bond Length (Å)	**Exp.**	**1**	**Bond Length (Å)**	**Exp.**	**2**	**Bond Length (Å)**	**Exp.**	**3**
O1-C12	1.238	1.231	O1-C11	1.243	1.239	O1-C12	1.240	1.239
O2-C14	1.239	1.222	O2-C13	1.226	1.222	O2-C14	1.223	1.222
O3-C31	1.331	1.357	O3-C29	1.330	1.356	C12-C13	1.475	1.482
O5-C31	1.211	1.212	O5-C29	1.210	1.208	C13-C14	1.470	1.482
N6-C19	1.334	1.346	N6-C17	1.337	1.339	N6-C19	1.333	1.341
N6-C21	1.410	1.401	N6-C19	1.422	1.406	N6-C21	1.402	1.401
C31-C22	1.493	1.482	C12-C13	1.482	1.480	C21-C22	1.392	1.402
C21-C22	1.414	1.419	C12-C17	1.394	1.388	C21-C29	1.398	1.404
Bond Angle (˚)	**Exp.**	**1**	**Bond Angle (˚)**	**Exp.**	**2**	**Bond Angle (˚)**	**Exp.**	**3**
C19-N6-C21	124.7	124.4	C17-N6-C19	125.9	127.8	C19-N6-C21	126.3	127.8
N6-C19-C13	127.3	127.5	N6-C17-C12	126.5	125.7	N6-C19-C13	125.2	125.6
O1-C12-C8	118.3	118.9	O1-C11-C8	118.1	118.3	O1-C12-C8	117.8	118.3
O1-C12-C13	118.9	119.3	O1-C11-C12	119.3	119.8	O1-C12-C13	119.9	119.8
C13-C12-C8	122.8	121.7	C8-C11-C12	122.6	121.8	C13-C12-C8	122.1	121.9
C12-C13-C14	123.3	122.6	C11-C12-C13	122.5	122.6	C12-C13-C14	122.0	122.5
O2-C14-C15	118.3	118.1	C17-C12-C11	120.2	119.3	O2-C14-C15	118.4	118.3
O2-C14-C13	121.6	122.2	C17-C12-C13	117.4	118.1	O2-C14-C13	122.1	122.3
O5-C31-C22	124.8	125.5	O2-C13-C12	122.2	122.4	C29-C21-N6	118.5	117.3
C12-C13-C19	120.0	119.5	O2-C13-C14	118.8	118.2	C12-C13-C19	119.5	119.4
Dihedral Angle (˚)	**Exp.**	**1**	**Dihedral Angle (˚)**	**Exp.**	**2**	**Dihedral Angle (˚)**	**Exp.**	**3**
N6-C21-C22-C23	178.5	178.8	O1-C11-C12-C17	0.0	0.0	O1-C12-C13-C14	-175.8	-179.5
N6-C21-C22-C31	-2.3	-1.8	C8-C11-C12-C13	0.0	0.0	N6-C21-C22-C24	179.6	179.9
N6-C21-C29-C27	-178.6	-178.5	C25-C23-C22-C19	180.0	180.0	C8-C12-C13-C19	-177.2	-179.6
C19-C13-C14-O2	176.1	178.3	C23-C22-C29-O3	180.0	180.0	C21-N6-C19-C13	178.5	179.6
C21-C22-C23-C25	0.1	0.4	C22-C20-C19-C27	0.0	0.0	C22-C21-C29-C27	0.7	0.2
C29-C21-C22-C31	178.0	177.7	C22-C23-C25-C27	0.0	0.0	C22-C24-C26-C27	0.2	0.1
C31-C22-C23-C25	-179.1	-179.1	C23-C22-C29-O5	0.0	0.0	C31-C26-C27-C29	178.5	179.9

3.2. Vibrational analysis

FT-IR spectroscopy is one of the most widespread methods used to identify the functional groups and bond structures of a particular molecule. However, a scaling factor is used to balance for the difference between experimental and theoretical vibrational frequencies. In this study, the computed frequencies were scaled with a factor of 0.983 for the 4000-1700 cm^{-1} region and 0.958 for the 1700-0 cm^{-1} region (Sundaraganesan et al., 2005). The FT-IR spectra of the studied isomers (**1-3**) obtained by quantum mechanical calculations are shown in Figure 2. In addition, for **1-3**, some selected computed approximate frequencies (unscaled and scaled) along with their IR intensities and probable assignments were exhibited in Table 2. The theoretical results are accompanied by experimental data (Halz et al., 2022).

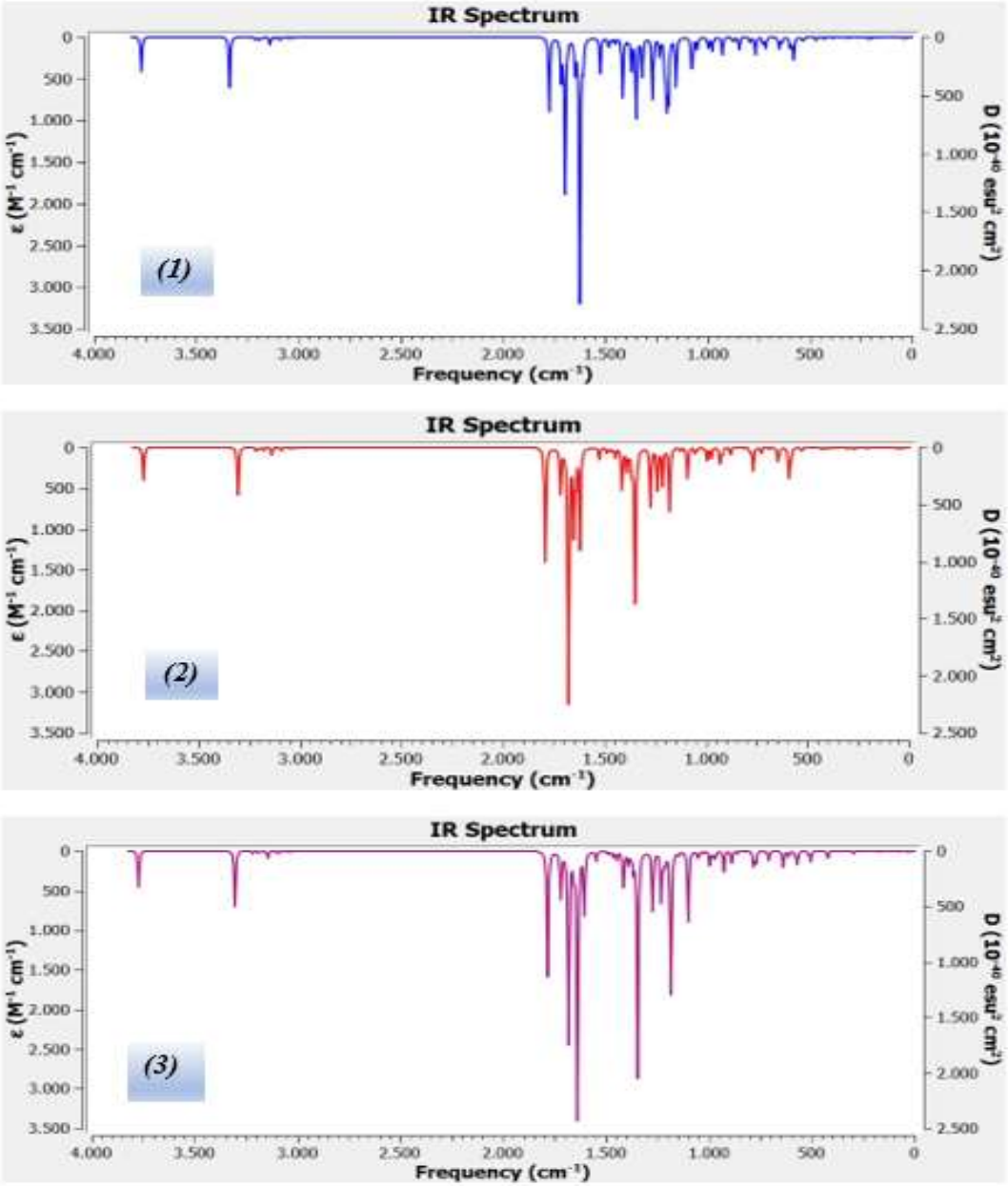

Figure 2. Theoretical FT-IR spectra of **1-3**

As demonstrated in Table 2, O-H and N-H stretching vibration modes were computed as 3768 cm^{-1} and 3336 cm^{-1} for compound **1**, 3769 cm^{-1} and 3303 cm^{-1} for compound **2**, and 3771 cm^{-1} and 3303 cm^{-1} for compound **3**, respectively. C-H stretching vibrations of the aromatic ring were predicted in the range of 3218-3173 cm^{-1} for **1**, 3214-3178 cm^{-1} for **2**, and 3217-3175 cm^{-1} for **3**. In addition, strong bands observed around 1650-1790 cm^{-1} in the theoretical spectra confirm the stretching motion of the carbonyl group. On the other hand, experimental results indicate that C=O stretching vibrations are observed in the region of 1647/1696 cm^{-1} for **1**, 1656/1704 cm^{-1} for **2**, and 1674 cm^{-1} for **3**. When the whole table is examined, it is evident that the experimental and theoretical results are compatible.

*Table 2. Experimental and computed approximate vibrational frequencies (in cm^{-1}) of compounds **1-3***

	1				**2**				**3**			
Assignment	**Exp.[a]**	**I_{IR}**	**Unscaled**	**Scaled**	**Exp.[a]**	**I_{IR}**	**Unscaled**	**Scaled**	**Exp.[a]**	**I_{IR}**	**Unscaled**	**Scaled**
νOH		120	3768	3704		118	3769	3705		133	3771	3707
νNH		176	3336	3279		169	3303	3247		203	3303	3247
νCH (Ar.)		2	3218	3163		11	3214	3159		10	3217	3162
νCH (Ar.)		9	3211	3156		2	3210	3155		1	3210	3155
νCH (Ar.)		1	3198	3144		3	3200	3146		1	3203	3149
νCH (Ar.)		10	3191	3137		3	3194	3140		7	3189	3135
νCH (Ar.)		5	3173	3119		11	3178	3124		3	3175	3121
$\nu_{as}CH_3$		11	3140	3087		10	3140	3087		10	3142	3089
$\nu_{as}CH_3$		16	3139	3086		15	3139	3086		16	3141	3088
$\nu_{as}CH_3$		5	3111	3058		3	3110	3057		3	3111	3058
$\nu_{as}CH_3$		11	3089	3036		11	3089	3036		10	3089	3036
νCH_3		5	3048	2996		4	3048	2996		4	3049	2997
νCH_3		6	3030	2978		5	3029	2978		5	3030	2978
νC=O		258	1773	1743		406	1790	1760		458	1783	1753
νC=O		138	1715	1686	1704	157	1716	1687		166	1718	1689
νC=O + νCN	1696	538	1696	1625		902	1678	1608		697	1681	1610
νCC + νC=O	1647	109	1647	1578	1656	289	1652	1583	1674	60	1656	1586
νCC + ipb HNC		917	1624	1556	1632	353	1620	1552	1628	974	1638	1569
νCC + ipb HCC	1552	124	1524	1460	1557	42	1525	1461	1586	35	1547	1482
δ CH_3	1492	11	1489	1426	1497	11	1489	1426		12	1489	1426
δ CH_3		2	1475	1413		5	1475	1413		1	1477	1415
δ CH_3 + ipb HCC		10	1465	1403		10	1464	1403		10	1465	1403
δ CH_3		20	1449	1388		34	1447	1386	1433	30	1447	1386
CH_3 umb. + ipb HCC	1405	208	1414	1355	1405	144	1415	1356		116	1414	1355
CH_3 umb. + ipb HCC		12	1391	1333		77	1389	1331	1390	42	1391	1333
ipb HCC + ipb HCN	1325	278	1348	1291	1347	492	1348	1291	1314	815	1345	1289
ipb HCC + ipb HCN	1144	169	1153	1105		227	1180	1130	1175	522	1184	1134
ipb HCC + νC-O	1077	68	1078	1033		11	1126	1079		259	1099	1053
ipb HCC + νC-O		72	1074	1029		110	1091	1045		22	1053	1009
opb HCC	978	3	978	937		2	996	954		1	994	952
opb HNC		47	976	935	979	38	975	934		15	980	939
ω CH_3	935	62	927	888		51	931	892	929	74	926	887
opb HCC	789	17	792	759	802	83	768	736	793	54	783	750

[a] Ref. (Halz et al., 2022) Abbreviations; I_{IR}: IR intensity, Ar: Aromatic; ν: symmetric stretching, ν_{as}: asymmetric stretching, ω: wagging, δ: scissoring, , umb: umbrella ipb: in plane bending, opb: out of plane bending

3.3. Thermodynamic parameters

Thermodynamic and physicochemical parameters of the studied isomers have been computed at 298.15 K. The results obtained from the calculations for vacuum, acetonitrile, and water phases at B3LYP/6-311++G (d, p) theory level are listed in Table 3. It was observed that the solvent phase dipole moment values for all three isomers were higher than those in the vacuum environment. The highest dipole moment values were calculated as 6.182 D (vacuum), 9.291 D (acetonitrile), and 10.638 D (water) for the ortho isomer (**1**). On the other side, the highest polarizability values were computed as 207.050 a. u. (vacuum), 288.190 a. u. (acetonitrile), and 302.480 a. u. (water) for the para isomer (**3**). Considering the thermodynamic state functions, it was observed that the positional isomerism did not cause significant changes in ΔE (total energy), ΔH (enthalpy), and ΔG (Gibbs free energy) values, as indicated in Table 3.

Table 3. The calculated thermodynamic and physicochemical quantities of studied isomers

1	**Vacuum**	**Acetonitrile**	**Water**
DM (Debye)	6.182	9.291	10.638
ΔE (a.u.)	-858.873	-858.903	-858.900
ΔH (a.u.)	-858.872	-858.902	-858.899
ΔG (a.u.)	-858.937	-858.967	-858.964
$\Delta E_{thermal}$ (kcal/mol)	161.581	161.229	161.071
$\Delta E_{vib.}$ (kcal/mol)	159.803	159.451	159.294
Cv (cal/molK)	63.900	63.925	64.025

$Cv_{vib.}$ (cal/molK)	57.939	57.963	58.064
S (cal/molK)	136.823	137.499	137.093
$S_{vib.}$ (cal/molK)	60.838	61.513	61.116
α (a.u.)	197.387	277.522	290.357
2	**Vacuum**	**Acetonitrile**	**Water**
DM (Debye)	2.977	4.687	5.268
ΔE (a.u.)	-858.878	-858.907	-858.904
ΔH (a.u.)	-858.877	-858.906	-858.903
ΔG (a.u.)	-858.940	-858.972	-858.968
$\Delta E_{thermal}$ (kcal/mol)	160.908	161.339	161.295
$\Delta E_{vib.}$ (kcal/mol)	159.131	159.562	159.517
Cv (cal/molK)	62.082	63.982	63.871
$Cv_{vib.}$ (cal/molK)	56.120	58.021	57.909
S (cal/molK)	131.468	139.343	137.996
$S_{vib.}$ (cal/molK)	55.177	63.051	61.705
α (a.u.)	199.448	276.755	289.285
3	**Vacuum**	**Acetonitrile**	**Water**
DM (Debye)	3.458	5.161	6.076
ΔE (a.u.)	-858.879	-858.909	-858.906
ΔH (a.u.)	-858.878	-858.908	-858.905
ΔG (a.u.)	-858.945	-858.975	-858.970
$\Delta E_{thermal}$ (kcal/mol)	161.536	161.264	161.218
$\Delta E_{vib.}$ (kcal/mol)	159.758	159.487	159.441
Cv (cal/molK)	64.051	64.154	64.067
$Cv_{vib.}$ (cal/molK)	58.089	58.192	58.106
S (cal/molK)	141.054	139.307	137.147
$S_{vib.}$ (cal/molK)	64.752	63.005	60.846
α (a.u.)	207.050	288.190	302.480

3.4. FMO and MEP analyses

HOMO functions as an electron donor as it is the outermost molecular orbital occupied with electrons while LUMO functions as electron acceptor as it is the first empty molecular orbital that is not occupied with electrons. Therefore, HOMO represents the ionization potential (I, I= - E_{HOMO}) of the molecule while LUMO represents the electron affinity (A, A= -E_{LUMO}) of the molecule. The energy range (ΔE = E_{LUMO}-E_{HOMO}) is chemical stability indicator of a particular molecule. Besides the energy gap, some quantum chemical reactivity identifiers (QCRI) such as chemical hardness, electronegativity, and back donation energy were calculated for vacuum, acetonitrile, and water environments. The results obtained are presented in Table 4. According to Table 4, among the o-, m- and p- isomers the highest ΔE value was calculated for the ortho isomer as 4.179 eV (water phase). Hence, the order of stability of the isomers is predicted as **1** > **2** > **3**. In addition, it was determined that the ΔE increased during the transitions from the gas phase to the solvent phase. As expected, a similar trend was also observed for chemical hardness values. Considering electrophilicity indexes (ω), the highest values were obtained in the vacuum phase and the order is as follows: **3** (5.273 eV) > **2** (4.991 eV) > **1** (4.720 eV). Similarly, the electronegativity values (χ) of studied compounds were estimated as **3** (4.608 eV) > **2** (4.501 eV) > **1** (4.399 eV) for vacuum environment. FMO theory analysis results revealed the effects of positional isomerism on reactivity indices.

Table 4. The computed QCRI values (in eV)

1	E_{HOMO}	E_{LUMO}	**ΔE**	**η**	**μ**	**χ**	**ω**	ω^+	ω^-	ΔN_{max}	$\Delta\varepsilon_{back}$
Vacuum	-6.449	-2.349	4.101	2.050	-4.399	4.399	4.720	2.776	7.176	2.146	-0.513
Acetonitrile	-6.246	-2.079	4.167	2.084	-4.163	4.163	4.158	2.337	6.499	1.998	-0.521
Water	-6.382	-2.203	4.179	2.090	-4.293	4.293	4.409	2.524	6.816	2.054	-0.522
2	E_{HOMO}	E_{LUMO}	**ΔE**	**η**	**μ**	**χ**	**ω**	ω^+	ω^-	ΔN_{max}	$\Delta\varepsilon_{back}$
Vacuum	-6.530	-2.472	4.059	2.029	-4.501	4.501	4.991	2.995	7.495	2.218	-0.507
Acetonitrile	-6.189	-2.079	4.110	2.055	-4.134	4.134	4.158	2.348	6.481	2.012	-0.514
Water	-6.319	-2.181	4.137	2.069	-4.250	4.250	4.366	2.500	6.749	2.055	-0.517
3	E_{HOMO}	E_{LUMO}	**ΔE**	**η**	**μ**	**χ**	**ω**	ω^+	ω^-	ΔN_{max}	$\Delta\varepsilon_{back}$
Vacuum	-6.621	-2.595	4.027	2.013	-4.608	4.608	5.273	3.221	7.829	2.289	-0.503
Acetonitrile	-6.252	-2.214	4.038	2.019	-4.233	4.233	4.437	2.573	6.806	2.097	-0.505
Water	-6.379	-2.335	4.044	2.022	-4.357	4.357	4.694	2.769	7.125	2.155	-0.505

The FMO distributions of studied isomers with DOS diagrams were depicted in Figure 3. The green color indicates negative lobes, and the red color indicates positive lobes. The HOMO and LUMO amplitudes of **1-3** are quite similar. HOMOs are dispersed throughout the molecules except for the methyl and carbonyl groups. Similarly, LUMOs are distributed throughout the molecules except the methyl groups.

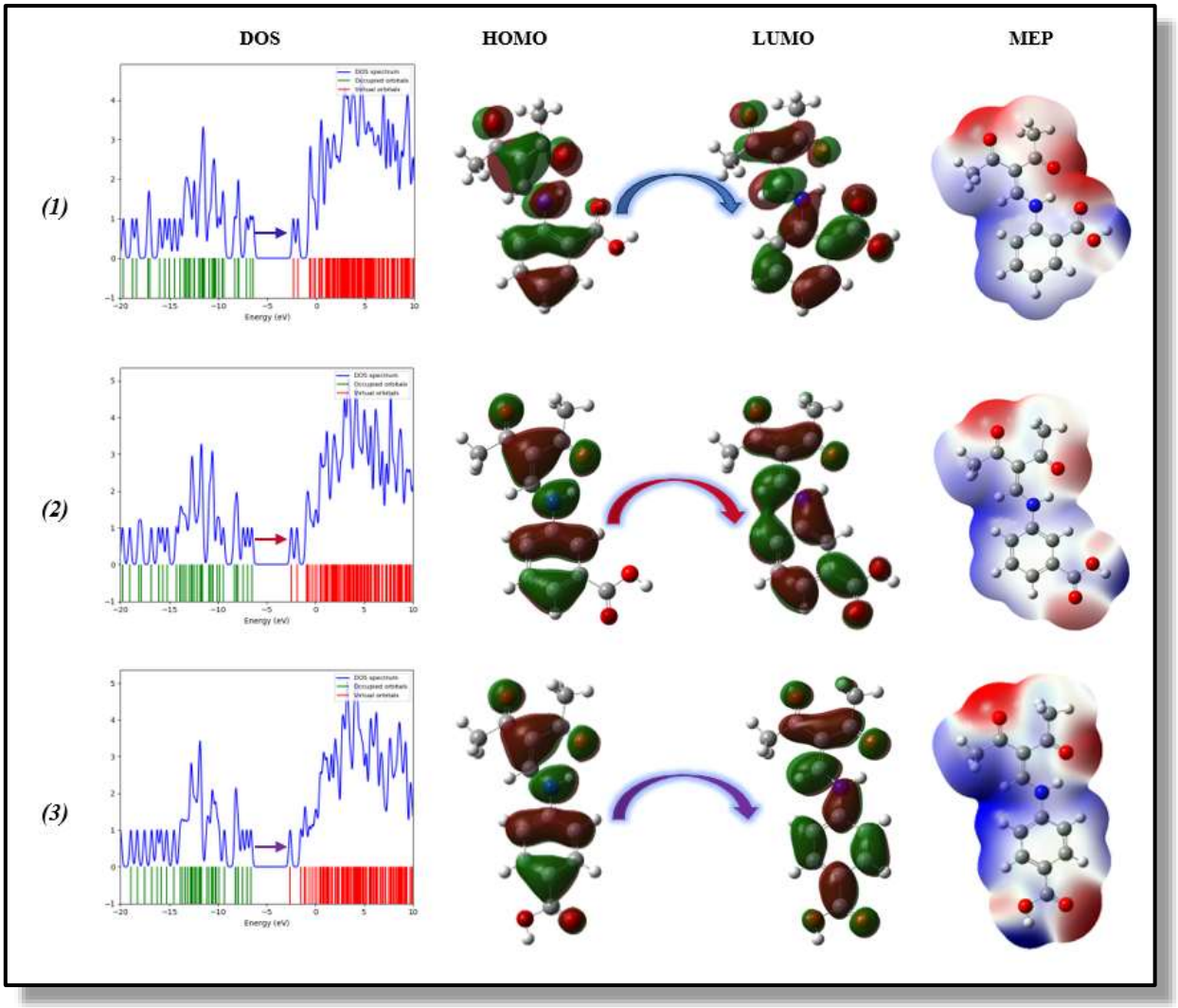

Figure 3. DOS, FMO (isoval:0.02) and MEP (isoval:0.0004) diagrams of **1-3**

Molecular electrostatic potential (MEP) mapping technique is used to better understand molecular interactions and provides important information about electron charge distribution or total charge density. In this part of the study, MEP maps have been visualized in order to clearly see the differences caused by positional isomerism in the electrostatic surface properties of compounds **1-3**. MEP diagrams are exhibited in Figure 3. The molecular electrostatic potentials of studied compounds are in the range of -0.0066 a. u. (deepest red) - +0.0066 a. u. (deepest blue) in vacuum. Generally, on the color scale of MEP maps, red designates high electron density, blue color indicates low electron density. That is, for each compound, a greater amount of electron density is observed around the oxygen atoms. Also, a lower amount of electron density was observed at the hydrogen surroundings and predominantly blue shading is present.

3.5. UV-Vis analysis

UV-Vis calculations of mentioned ortho (**1**), meta (**2**) and para (**3**) derivatives were carried out using TD-DFT/B3LYP/6-311++G (d, p) methodology in acetonitrile and water medium (casida et al., 1988; Scalmani et al., 2006; Van Caillie and Amos, 1999; Adamo and Jacquemin, 2013). Figure 4 presents computed absorption spectra of **1-3** in acetonitrile. In addition, theoretical UV-Vis analysis outputs (computed absorption wavelengths (λ_{calc}), excitation energies (ΔE), oscillator strengths (*f*) and major contributions) are given in Table 5. As demonstrated in Table 5, it was defined that the calculated peaks for compounds **1-3** at about 342 nm were caused by

H→L (70% MO contribution) electronic transitions. Besides, the second states S_2 correspond to H-1→ L and H-1→L+1 electronic transitions.

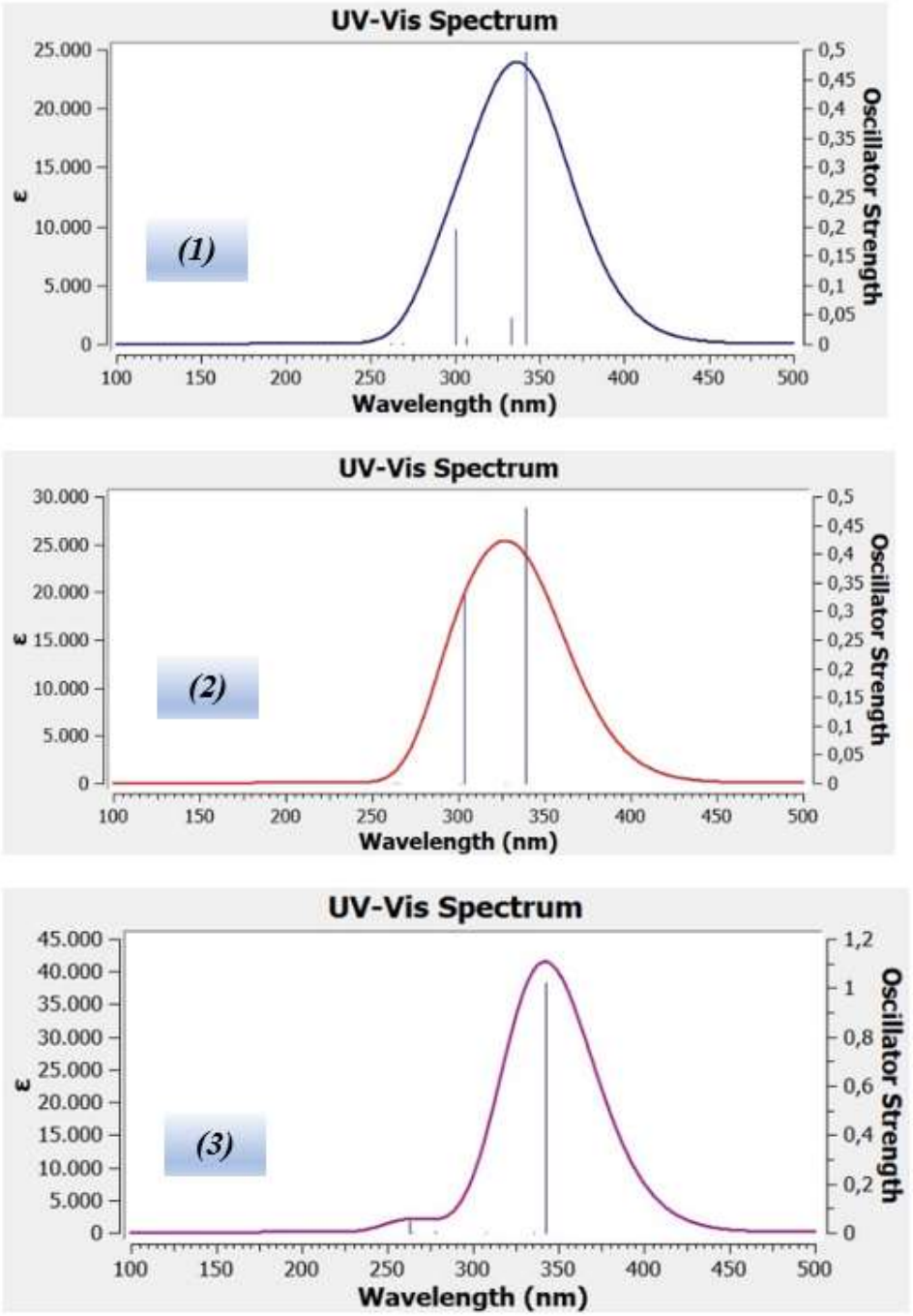

Figure 4. Computed UV-vis spectra of **1-3** in acetonitrile

*Table 5. UV-Vis analysis results of **1-3***

1	**Medium**	**ES**	**$\lambda_{calc.}$ (nm)**	**ΔE (eV)**	***f***	**Major Contributions (H=HOMO, L=LUMO)**
	Water	S_1	341.74	3.6280	0.4992	H→L (67%)
		S_2	332.40	3.7300	0.0389	H-1→L (62%), H-1→L+1 (21%)
		S_3	306.05	4.0511	0.0129	H-2→L (53%), H→L+1 (28%), H-1→L+2 (27%)
		S_4	299.93	4.1338	0.1915	H→L+1 (61%), H-2→L (24%)
		S_5	268.13	4.6240	0.0024	H-1→L+1 (60%), H-1→L (23%)
		S_6	262.08	4.7309	0.0016	H-1→L+2 (59%), H-2→L (31%)
	Acetonitrile	S_1	342.00	3.6253	0.4958	H→L (67%)
		S_2	333.03	3.7229	0.0440	H-1→L (62%), H-1→L+1(21%)
		S_3	306.57	4.0443	0.0111	H-1→L (54%), H-1→L+2 (27%), H→L+1(27%)
		S_4	300.20	4.1300	0.1952	H→L+1(62%), H-2→L (23%)
		S_5	268.71	4.6141	0.0024	H-1→L+1 (61%), H-1→L (24%)
		S_6	262.19	4.7288	0.0016	H-1→L+2 (59%), H-1→L (31%)
2	**Medium**	**ES**	**$\lambda_{calc.}$ (nm)**	**ΔE (eV)**	***f***	**Major Contributions (H=HOMO, L=LUMO)**
	Water	S_1	338.92	3.6582	0.4773	H→L (67%)
		S_2	326.42	3.7983	0.0000	H-1→L (62%), H-1→L+1 (25%)
		S_3	303.50	4.0851	0.3366	H→L+1 (68%)
		S_4	301.12	4.1175	0.0006	H-2→L (56%), H-2→L+1 (27%), H-1→L+2 (29%)
		S_5	264.85	4.6813	0.0001	H-1→L+2 (52%), H-1→L+1 (30%), H-1→L (28%)
		S_6	262.38	4.7254	0.0001	H-1→L+1(55%), H-1→L+2 (33%), H-2→L (25%)
	Acetonitrile	S_1	339.17	3.6555	0.4809	H→L (70%)
		S_2	327.04	3.7911	0.0000	H-1→L (62%), H-1→L+1 (25%)
		S_3	303.55	4.0844	0.3354	H→L+1 (68%)
		S_4	301.58	4.1112	0.0006	H-2→L (56%), H-2→L+1(27%), H-1→L+2 (29%)
		S_5	265.06	4.6777	0.0001	H-1→L+2 (50%), H-1→L+1(31%), H-1→L (29%)
		S_6	262.62	4.7211	0.0001	H-1→L+1(54%), H-1→L+2 (35%), H-2→L (25%)
3	**Medium**	**ES**	**$\lambda_{calc.}$ (nm)**	**ΔE (eV)**	***f***	**Major Contributions (H=HOMO, L=LUMO)**
	Water	S_1	342.04	3.6248	1.0196	H→L (70%)
		S_2	335.27	3.6980	0.0007	H-1→L (66%)
		S_3	306.98	4.0388	0.0006	H-2→L (61%), H-1→L+2 (23%)
		S_4	278.25	4.4559	0.0046	H-3→L (54%), H→L+1 (30%), H→L+3 (25%)
		S_5	264.63	4.6852	0.0003	H-1→L+2 (56%), H-1→L+3 (30%), H-2→L (23%)
		S_6	263.03	4.7138	0.0450	H→L+1 (58%), H-3→L (26%), H-4→L (23%)
	Acetonitrile	S_1	342.29	3.6222	1.0214	H→L (70%)
		S_2	335.84	3.6918	0.0008	H-1→L (66%)
		S_3	307.42	4.0330	0.0006	H-2→L (62%), H-1→L+2 (22%)
		S_4	278.24	4.4560	0.0046	H-3→L (54%), H→L+1 (30%), H→L+3 (25%)
		S_5	264.75	4.6831	0.0003	H-1→L+2 (56%), H-1→L+3 (31%), H-2→L (23%)
		S_6	263.01	4.7140	0.0452	H→L+1 (58%), H-3→L (26%), H-4→L (22%)

3.6. NBO study

In this section, NBO studies were carried out to evaluate the charge transfer and electronic transitions between donor and acceptor fragments of studied compounds. To this end, possible intramolecular interactions were examined for compounds **1-3** and the stabilization energy values corresponding to these interactions were computed and listed in Table 6. Stabilization energies greater than 10 kcal/mol are taken into account. LP represents lone pairs. See the atomic numbering in Figure 1 for selected NBO pairs. As indicated in Table 6, similar interactions were determined for all three isomers. These interactions are $\pi \rightarrow \pi^*$, LP $\rightarrow \pi^*$, and LP $\rightarrow \sigma^*$ interactions with stabilization energies varying between 12.64-62.54 kcal/mol. The highest stabilization energy values were calculated for LP (2) O3 (ED_i = 1.83139e) $\rightarrow \pi^*$ (O5-C31) (ED_j = 0.25883e) (**1**; 42.51 kcal/mol), LP (1) N6 (ED_i = 1.56865e) $\rightarrow \pi^*$ (C12-C17) (ED_j = 0.31229e) (**2**; 57.23 kcal/mol), and LP (1) N6 (ED_i = 1.56546e) $\rightarrow \pi^*$ (C13-C19) (ED_j = 0.30155e) (**3**; 62.54 kcal/mol) interactions. Considering C-C ($\pi \rightarrow \pi^*$) resonance energies, the stabilization energies of π (C23-C25) $\rightarrow \pi^*$ (C27-C29) and π (C27-C29) $\rightarrow \pi^*$ (C23-C25) interactions for the ortho isomer (**1**) were determined as 23.32 kcal/mol and 16.12 kcal/mol, respectively. For meta (**2**) and para (**3**) isomers, these values vary between 17.65-21.04 kcal/mol and 16.65-24.26 kcal/mol.

*Table 6. Main findings of the NBO study for **1-3***

	Donor(i)	ED_i/e	Acceptor(j)	ED_j/e	$E^{(2)}$ kcal/mol	E(j)-E(i)/a.u	F(i.j)/a.u
1	π N6-C21	1.75262	π* C13-C19	0.28834	34.67	0.35	0.099
	π C13-C19	1.75475	π* O1-C12	0.18498	21.90	0.30	0.073
			π* O2-C14	0.18728	24.86	0.30	0.078
	π C23-C25	1.65976	π* C27-C29	0.31690	23.32	0.28	0.072
	π C27-C29	1.68171	π* N6-C21	0.78265	34.95	0.21	0.088
			π* C23-C25	0.29923	16.12	0.29	0.062
	LP (2) O1	1.89074	σ* C8-C12	0.04432	17.90	0.68	0.100
			σ* C12-C13	0.05997	15.06	0.73	0.094
	LP (2) O2	1.89200	σ* C13-C14	0.06026	17.89	0.71	0.102
			σ* C14-C15	0.05594	19.89	0.63	0.101
	LP (2) O3	1.83139	π* O5-C31	0.25883	42.51	0.34	0.111
	LP (2) O5	1.84831	σ* C22-C31	0.06070	15.87	0.70	0.096
	Donor(i)	**ED_i/e**	**Acceptor(j)**	**ED_j/e**	**$E^{(2)}$ kcal/mol**	**E(j)-E(i)/a.u**	**F(i.j)/a.u**
2	π C12-C17	1.73987	π* O1-C11	0.21245	25.07	0.29	0.077
			π* O2-C13	0.18943	25.19	0.30	0.079
	π C19-C27	1.63222	π* C20-C22	0.36696	19.66	0.29	0.068
			π* C23-C25	0.30787	17.65	0.33	0.069
	π C20-C22	1.66113	π* O5-C29	0.23883	20.06	0.27	0.068
			π* C19-C27	0.39684	20.20	0.28	0.068
			π* C23-C25	0.30787	18.53	0.32	0.069
	π C23-C25	1.64077	π* C19-C27	0.39684	21.04	0.27	0.068
			π* C20-C22	0.36696	21.01	0.28	0.068
	LP (2) O1	1.88676	σ* N6-H7	0.05484	13.97	0.68	0.088
			σ* C8-C11	0.04144	16.78	0.70	0.099
			σ* C11-C12	0.05657	12.64	0.75	0.088
	LP (2) O2	1.89135	σ* C12-C13	0.06090	18.08	0.71	0.102
			σ* C13-C14	0.05573	19.86	0.63	0.101
	LP (2) O3	1.82847	π* O5-C29	0.23883	43.05	0.35	0.111
	LP (2) O5	1.84957	σ* O3-C29	0.09659	33.42	0.61	0.129
			σ* C22-C29	0.06642	17.41	0.69	0.100
	LP (1) N6	1.56865	π* C12-C17	0.31229	57.23	0.28	0.116
			π* C19-C27	0.39684	37.79	0.28	0.093
	Donor(i)	**ED_i/e**	**Acceptor(j)**	**ED_j/e**	**$E^{(2)}$ kcal/mol**	**E(j)-E(i)/a.u**	**F(i.j)/a.u**
3	π C13-C19	1.74374	π* O1-C12	0.20861	24.59	0.29	0.076
			π* O2-C14	0.18540	24.67	0.30	0.079
	π C21-C22	1.62823	π* C24-C26	0.38223	24.26	0.29	0.075
			π* C27-C29	0.28382	15.02	0.30	0.061
	π C24-C26	1.63396	π* O5-C31	0.25123	22.33	0.27	0.071
			π* C21-C22	0.40301	17.71	0.27	0.062
			π* C27-C29	0.28382	22.00	0.28	0.072
	π C27-C29	1.67678	π* C21-C22	0.40301	23.27	0.27	0.073
			π* C24-C26	0.38223	16.65	0.28	0.062
	LP (2) O1	1.88662	σ* N6-H7	0.05541	13.97	0.68	0.088
			σ* C8-C12	0.04130	16.77	0.70	0.099
			σ* C12-C13	0.05694	12.73	0.75	0.088
	LP (2) O2	1.89134	σ* C13-C14	0.06132	18.21	0.71	0.102
			σ* C14-C15	0.05543	19.23	0.64	0.100
	LP (2) O3	1.83308	π* O5-C31	0.25123	41.98	0.35	0.110
	LP (1) N6	1.56546	π* C13-C19	0.30155	62.54	0.25	0.116
			π* C21-C22	0.40301	44.53	0.26	0.096

4. Conclusion

Herein, the main findings as a result of quantum chemical calculations on the mentioned isomers are discussed. The DFT study results show that computed geometrical parameters and vibrational frequencies are in good agreement with experimental values. Examination of the dihedral angles reveals that molecules **1** and **3** exhibit nearly planar structures, while molecule **2** exhibits an exact planar structure. It was determined that the values of thermodynamic state functions for all three isomers were slightly different from each other. Therefore, it can be concluded that the effect of positional isomerism on ΔE (total energy), ΔH (enthalpy) and ΔG (Gibbs free energy) values is quite small. On the other side, it was observed that the calculated DFT-based reactivity descriptors had similar tendencies for the gas and solvent phases. According to the results, among the *o-, m-* and *p-* isomers the highest ΔE value was calculated for the ortho isomer as 4.179 eV (water phase). Hence, the order of stability of the isomers is predicted as **1 > 2 > 3.** From the TD-DFT results, it can be concluded that the peaks are predominantly due to π→π* and n→π* transitions. In addition, the three-dimensional visualization of MEP surfaces allowed the identification of reactive and possible interaction zones of the isomers of interest. Considering the successful applications of the studied compound class in medicinal chemistry, the drug-like properties of the relevant derivatives can be investigated in further studies. With the support of the data presented in this study, structure-activity relationships can be determined and utilized in drug design studies.

5. Acknowledgement

The numerical calculations reported in this paper were fully performed at TUBITAK ULAKBIM, High Performance and Grid Computing Center (TRUBA resources).

References

Aadhityan A., Preferencial Kala C., John Thiruvadigal D (2021). Theoretical investigation of spin-dependent electron transport properties of dibromobenzene based positional isomers, Computational Materials Science, 187, 110109.

Adamo C., Jacquemin D. (2013). The calculations of excited-state properties with time-dependent density functional theory, Chemical Society Reviews, 42, 845–856. https://doi.org/10.1039/C2CS35394F

Ardakani A. A., Kargar H., Feizi N., Tahir M. N. (2018). Synthesis, characterization, crystal structures and antibacterial activities of some Schiff bases with N2O2 donor sets, Journal of Iranian Chemical Society, 15, 1495–1504. http://dx.doi.org/10.1007/s13738-018-1347-6

Becke A.D. (1993). A new mixing of Hartree–Fock and local density-functional theories, Journal of Chemical Physics, 98, 1372–1377. https://doi.org/10.1063/1.464304.

Becke A.D. (1993). Density-functional thermochemistry. III. The role of exact exchange, Journal of Chemical Physics, 98, 5648–5652. https://doi.org/10.1063/1.464913

Casida M.E., Jamorski C., Casida K.C., Salahub D.R. (1998). Molecular excitation energies to high-lying bound states from time-dependent density-functional response theory: characterization and correction of the time-dependent local density approximation ionization threshold, Journal of Chemical Physics, 108, 4439–4449. https://doi.org/10.1063/1.475855.

Chen F., Wang Y., Song S., Wang K., Zhang, Q. (2023). Impact of Positional Isomerism on Melting Point and Stability in New Energetic Melt-Castable Materials, Journal of Physical Chemistry. 127, 8887−8893 https://doi.org/10.1021/acs.jpcc.3c01554

Dennington R., Keith T.A., Millam J.M. (2016). GaussView, Version 6 Semichem Inc., Shawnee Mission, KS.

Eliel E. L., Wilen, S. H. Stereochemistry of Organic Compounds, 1st ed.; Wiley-Interscience: New York, 1994.

Frisch M. J., Trucks G.W., Schlegel H. B., Scuseria G.E. et.al. (2016). Gaussian 16 Rev. B.01, Wallingford, CT.

Gazquez, J. L., Cedillo, A., Vela, A. (2007). Electrodonating and electroaccepting powers, Journal of Physical Chemistry A, 111(10), 1966-1970. https://doi.org/10.1021/jp065459f

Gogoi H. P., Singh A., Barman P., Choudhury D. (2022). A new potential ONO Schiff-Base ligand and its Cu(II), Zn(II) and Cd(II) complexes: Synthesis, structural elucidation, theoretical and bioactivity studies, Inorganic Chemistry Communications, 146, 110153. https://doi.org/10.1016/j.inoche.2022.110153

Gomez, B., Likhanova, N. V., Domínguez-Aguilar, M. A., Martínez-Palou, R., Vela, A., Gazquez, J. L. (2006). Quantum chemical study of the inhibitive properties of 2-pyridyl-azoles, Journal of Physical Chemistry B, 110(18), 8928-8934. https://doi.org/10.1021/jp057143y

Halz J. H., Hentsch A., Wagner C., Merzweiler K. (2022). Synthesis and crystal structures of three Schiff bases derived from 3-formylacetylacetone and o-, m- and p-aminobenzoic acid Acta Crystallographica Section E: Crystallographic Communications, E78, 54–59. https://doi.org/10.1107/S2056989021013050

Herzberg G. (1964). Molecular Spectra and Molecular Structure III, 1. Edition, D. Van Nostrand Company, Inc., New York.

Hill T. L. (1962). An Introduction to Statistical Thermodynamics, Addison- Wesley Publishing, Inc, London.

Koopmans T. (1934). Über die zuordnung von wellenfunktionen und eigenwerten zu den einzelnen elektronen eines atoms, Physica, 1–6, 104–113. https://doi.org/10.1016/S0031-8914(34)90011-2

Lee C., Yang W., Parr R.G. (1988). Development of the Colle-Salvetti correlation-energy formula into a functional of the electron density, Physical Review B, 37, 785–789. https://doi.org/10.1103/PhysRevB.37.785

Marenich A.V., Cramer C.J., Truhlar D.G. (2009). Universal solvation model based on solute electron density and on a continuum model of the solvent defined by the bulk dielectric constant and atomic surface tensions, Journal of Physical Chemistry B., 113 (18), 6378-6396. https://doi.org/10.1021/jp810292n

McQuarrie D.A. (1973). Statistical Thermodynamics, Harper & Row Publishers, New York.

Niu M., Cao Z., Xue R., Wang S., Dou J., Wang D. (2011). Structural diversity of Cu(II) compounds of Schiff bases derived from 2-hydroxy-1-naphthaldehyde and a series of aminobenzoic acid, Journal of Molecular Structure, 996, 101–109. http://dx.doi.org/10.1016/j.molstruc.2011.04.025

O'Boyle N. M., Tenderholt A. L. Langer K. M. (2008). Cclib: a library for package-independent computational chemistry algorithms, Journal of computational chemistry, 29 (5), 839-45. https://doi.org/10.1002/jcc.20823

Parr R.G. (1999). Electrophilicity index, Journal of American Chemical Society, 121,1922-1924. https://doi.org/10.1021/ja983494x

Parr R.G., Pearson R.G. (1983). Absolute hardness: companion parameter to absolute electronegativity, Journal of American Chemical Society, 105, 7512-7516. https://doi.org/10.1021/ja00364a005

Pearson R.G. (1986). Absolute electronegativity and hardness correlated with molecular orbital theory, Proceedings of the National Academy of Sciences of the United States of America, 83, 8440-8441. https://doi.org/10.1073/pnas.83.22.8440

Perdew J.P., Levy M. (1983). Physical content of the exact kohn-sham orbital energies: band gaps and derivative discontinuities, Physical Review Letters, 51, 1884-1887. https://doi.org/10.1103/PhysRevLett.51.1884

Perdew J.P., Parr R.G., Levy M., Balduz J.L. (1982). Density-functional theory for fractional particle number: derivative discontinuities of the energy, Physical Review Letters, 49, 1691. https://doi.org/10.1103/PhysRevLett.49.1691.

Reed A.E., Curtiss L.A., Weinhold F. (1988). Intermolecular interactions from a natural bond orbital, donor-acceptor viewpoint, Chemical Reviews. 88(6), 899-926, https://doi.org/10.1021/cr00088a005.

Scalmani G., Frisch M.J., Mennucci B., Tomasi J., Cammi R., Barone V. (2006). Geometries and properties of excited states in the gas phase and in solution: theory and application of a time-dependent density functional theory polarizable continuum model, Journal of Chemical Physics, 124, 1–15. https://doi.org/10.1063/1.2173258.

Serdaroğlu G., Durmaz S. (2010). DFT and statistical mechanics entropy calculations of diatomic and polyatomic molecules, Indian Journal of Chemistry, 49, 861–866.

Singh A., Gogoi H. P., Barman P. (2022). Comparative study of palladium (II) complexes bearing tridentate ONS and NNS Schiff base ligands: Synthesis, characterization, DFT calculation, DNA binding, bioactivities, catalytic activity, and molecular docking, Polyhedron, 115895. https://doi.org/10.1016/j.poly.2022.115895

Sundaraganesan N., Ilakiamani S., Salem H., Wojciechowski P.M., Michalska D. (2005). FT-Raman and FT-IR spectra, vibrational assignments and density functional studies of 5-bromo-2-nitropyridine, Spectrochim. Acta A Mol. Biomol. Spectrosc., 61, 2995–3001. https://doi.org/10.1016/j.saa.2004.11.016.

Tadele K.T., Tsega T.W. (2019). Schiff Bases and their metal complexes as potential anticancer candidates: a review of recent works, Anti-Cancer Agents Med, Chem. (Formerly Curr. Med. Chem. Agents), 19 1786–1795. http://dx.doi.org/10.2174/1871520619666190227171716

Van Caillie C., Amos R.D. (1999). Geometric derivatives of excitation energies using SCF and DFT, Chemical Physics Letters, 308, 249–255. https://doi.org/10.1016/S0009-2614(99)00646-6.

Vyas A., Koshti R.R., Patel H.N., Sangani C.B., Prajapati A.K., Yao Y., Duan, Y.T. (2022). Mesomorphic behaviour, optical and quantum computational study:Effect of electron density on newly synthesized liquid crystalline positional isomers, Journal of Molecular Liquids, 349, 118142. https://doi.org/10.1016/j.molliq.2021.118142

Weinhold F., Landis C.R., Glendening E.D. (2016). What is NBO analysis and how is it useful, International Reviews in Physical Chemistry, 35, 399-440. https://doi.org/10.1080/0144235X.2016.1192262.

Yin H., Liu H., Hong M. (2012). Synthesis, structural characterization and DNA-binding properties of organotin(IV) complexes based on Schiff base ligands derived from 2-hydroxy-1-naphthaldy and 3- or 4-aminobenzoic acid, Journal of Organometallic Chemistry, 713, 11-19. http://dx.doi.org/10.1016/j.jorganchem.2012.03.027